Journal of the European Ceramic Society **11** (1993) 417–424

Bending Fatigue Behavior of Nuclear-grade Graphite under Impact Loading

Masatoshi Futakawa, Kenji Kikuchi, Yasusi Muto

Department of High Temperature Engineering, Tokai Research Establishment, Japan Atomic Energy Research Institute, Tokai-mura, Ibaraki-ken, 319-11 Japan

&

Heki Shibata

Institute of Industrial Science, University of Tokyo, Tokyo, 106 Japan

(Received 16 March 1992: revised version received 17 August 1992: accepted 30 September 1992)

Abstract

The graphite components in an HTR (high-temperature gas-cooled reactor) are subjected to impact forces due to earthquake. It is important from the viewpoint of seismic safety design to investigate the difference of strength under impact loading and nonimpact loading.

Both bending strength and bending fatigue strength tests, therefore, were carried out under impact and nonimpact loading on two kinds of graphite materials: isotropic and near-isotropic. The impact response analyses, which used a beam model taking account of the contact behavior between specimen and tup, were performed to evaluate the relationships between impact energy, impact force and stress.

The main conclusions obtained are summarized as follows:

(1) A beam model taking account of the contact behavior through the Hertzian theory is applicable to describe the impact behavior.
(2) The bending strength of graphite is independent of strain rate in the range from 10^{-6} to 5/s.
(3) The bending fatigue strength of graphite is lower under impact loading than under non-impact, independent of the specimen volume and type of graphite.

Die Graphitkomponenten eines HTR (Gasgekühlter Hochtemperaturreaktor) unterliegen im Falle eines Erdbebens beträchtlichen Stoßkräften. Vom Standpunkt seismischer Sicherheit aus ist es daher wichtig, den Unterschied der Festigkeit bei Stoßbeanspruchung und stoßfreier Beanspruchung zu untersuchen.

Deshalb wurden für zwei verschiedene Graphitwerkstoffe Versuche zur Biegefestigkeit und zum Ermüdungsverhalten unter Biegebeanspruchung durchgeführt. Vollständig isotrope und nahezu isotrope Werkstoffe wurden hierbei untersucht. Um den Zusammenhang zwischen der Stoßenergie, der StoBkraft und der Spannung zu klären, wurde das Materialverhalten bei Stoßeinwirkung genau analysiert. Die Analyse beruht auf einem Balkenmodell und berücksichtigt das Kontaktverhalten zwischen Probe und Druckkopf.

Als wichtigste Ergebnisse können genannt werden:

(1) Ein Balkenmodell, das das Kontaktverhalten gemäß der Hertz'schen Theorie berücksichtigt, kann erfolgreich zur Beschreibung des Materialverhaltens bei StoBbeanspruchung angewendet werden.
(2) Im Bereich zwischen 10^{-6} bis 5/s hängt die Biegefestigkeit von Graphit nicht von der Belastungsgeschwindigkeit ab.
(3) Unter ermüdender Beanspruchung ist die Festigkeit von Graphit unter Stoßeinwirkung geringer als für den Fall stoßfreier Beanspruchung, wobei dieses Verhalten unabhängig vom Probenvolumen und der Art des Graphits ist.

Les composants en graphite d'un HTR (réacteur à haute température refroidi par gaz) sont soumis à des

Journal of the European Ceramic Society 0955-2219/93/$6.00

forces d'impacts engendrées par les tremblements de terre. Il est important pour la prévision de la sécurité sismique d'étudier la différence de résistance entre la mise en charge sous impact et sans impact. Dès lors, les auteurs ont mesuré la résistance à la flexion et à la flexion en fatigue, sous impact et sans impact, sur deux types de matériaux en graphite: l'un isotrope et l'autre proche de l'isotropie.

Des analyses de la réponse à l'impact, qui utilisent un modèle tenant compte du comportement lors du contact entre l'échantillon et la tête du marteau, ont été menées, pour évaluer les relations entre énergie d'impact, force d'impact et contrainte.

Les conclusions générales auxquelles les auteurs sont parvenus peuvent se résumer comme suit:

(1) On peut appliquer valablement un modèle, tenant compte du comportement lors du contact, issu de la théorie Hertzlenne, pour décrire le comportement à l'impact.

(2) La résistance à la flexion du graphite est indépendante de la vitesse d'élongation dans la gamme 10^{-6} à 5/s.

(3) La résistance à la flexion en fatigue du graphite est plus faible sous l'effet d'un impact que sans impact, indépendamment du volume de l'échantillon traité et du type de graphite.

1 Introduction

The core of the HTR (high-temperature gas-cooled reactor) consists of many kinds of graphite components: fuel block, reflector block, dowel, key, etc.[1] These components are repeatedly subjected to impact forces due to collision motion during earthquakes. Accordingly, it is important from the viewpoint of a seismic safety design in the HTR to make clear the impact strength and the impact fatigue behavior of the graphites.

Hitherto, the impact fatigue tests for an isotropic graphite IG-11, had been carried out by using a pendulum-type impact repeatedly bending machine. Then, the relation between impact energy and the stress generated by impact was discussed through the analysis, using the simple one-dimensional model, taking the Hertzian contact stiffness into consideration.[2] As a result, it had been confirmed that the endurance curves evaluated using a maximum stress induced by impact are independent of the specimen size, and that the fatigue strength of IG-11 is lower in impact than in nonimpact.

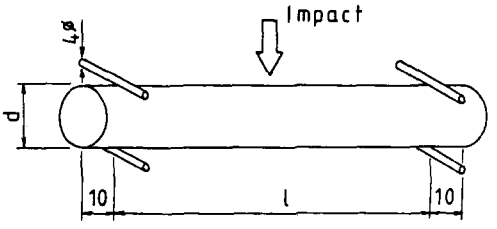

Fig. 1. Specimen shape. Specimen size: *S*, $l = 110$ mm, $d = 10$ mm; *M*, $l = 210$ mm, $d = 10$ mm; *L*, $l = 210$ mm, $d = 20$ mm.

Additionally, the impact fatigue behavior and the impact bending strength of another kind of nuclear-grade graphite, that is, a near-isotropic graphite PGX, were investigated and compared with those of IG-11. The impact response analyses were conducted using a finite element method in order to discuss the effect of higher vibrational modes of the beam specimen on the stress generated by impact.

2 Experimental Method

The impact fatigue and the impact strength tests were carried out using the pendulum-type impact repeatedly bending machine.[2] The maximum impact velocity, energy and cyclic frequency are 3 m/s, 1 J and 0·5 Hz respectively. The impact force acting on the specimen was measured from a strain gage instrumented tup, of which the radius of contact surface is 5 mm. The specimen was simply supported at each end and centrally subjected to impact as shown in Fig. 1. The size of specimen was varied to investigate the volume effect on the strength, that is *S* denotes that $l = 110$ mm and $d = 10$ mm, *M* that $l = 210$ mm and $d = 10$ mm, and *L* that $l = 210$ mm and $d = 20$ mm. The strain at the outer fiber of the specimen was measured by using the strain gage which was fixed at its center across the impact point. The quasi-static three-point bending fatigue tests were performed under cyclic stress in unidirectional bending by using an electrohydraulic testing machine. In the quasi-static fatigue tests, the frequency of cyclic load was 1 Hz at a triangular wave.

The mechanical properties of graphite materials are shown in Table 1.

Table 1. Mechanical properties of graphite material

	IG-11	*PGX* (//)	*PGX* (⊥)
Bending strength (MPa)	40·3 (2·3)	14·5 (0·4)	16·5 (1·4)
Young's modulus (GPa)	10·7 (0·7)	6·3 (0·1)	7·6 (0·07)
Poisson's ratio	0·18 (0·03)	0·09 (0·01)	0·07 (0·01)

Number of specimens: 5 (PGX), 15 (IG-11).
Standard deviation in parentheses.

3 Analytical Method

The simple analytical model taking account of the Hertzian contact theory had been proposed to investigate the relation between the stress generated by impact, the impact force, and the damping effect under the impact velocity.[2] The model, however, could not represent the higher vibrational modes of the specimen which might affect the generated stress. Thereupon, the impact response analysis was performed by using the beam model, as shown in Fig. 2, in which the contact stiffness used to describe the contacting behavior between the tup and the specimen was derived from the Hertzian theory[3] as in the following equation:

$$F(t) = k_H X(t)^{3/2} \tag{1}$$

where $X(t)$ is the distance moved by the impactor into the target because of local compressive deformation at the point of contact. When two cylinders with radii r_1 and r_2 are placed in contact normally to each other, the Hertzian contact stiffness k_H of the two cylinders is given by

$X(t) >= 0$

$$k_H = \frac{4\alpha}{3(\delta_1 + \delta_2)\sqrt{1/2r_1 + 1/2r_2}} \tag{2}$$

$$\delta_i = (1 - \nu_i^2)/E_i\pi$$

and

$X(t) < 0$

$$k_H = 0 \tag{3}$$

where ν is Poisson's ratio, E the modulus of elasticity, and α a constant defined by r_1/r_2.

Additionally, the dimensions of the ellipse of the contact area can be expressed by using k_H as

$$a = \frac{\beta}{\sqrt{1/2r_1 + 1/2r_2}} \sqrt[3]{F/k_H} \tag{4}$$

$$b = \frac{\gamma}{\sqrt{1/2r_1 + 1/2r_2}} \sqrt[3]{F/k_H} \tag{5}$$

where a and b are the semi-major and semi-minor axes of the contact ellipse, respectively, and β and γ are constants defined by r_1/r_2.

It is essential for evaluating the relation between impact energy, impact force and stress to take account of the effect of the damping factor on the impact response. Unfortunately, the damping behavior results from so complicated a phenomenon that it can not be analytically represented yet. Therefore, the damping factor measured experimentally by using the FFT analyzer was adopted for the beam model.

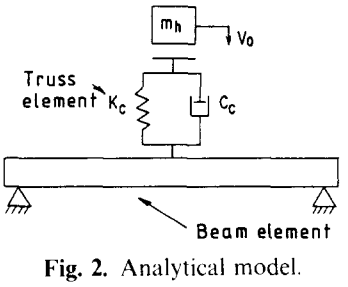

Fig. 2. Analytical model.

4 Results and Discussion

4.1 Impact response

Figure 3 shows the impact responses of the force and the strain in the IG-11 specimens. The high-frequency components are superimposed on both the force and the strain because of the impact behavior affected by the interaction between specimen and tup. Especially in the case of the *L*-type specimen, the effect of the inertia of the specimen on the impact response is so conspicuous that the maximum force and the maximum strain do not occur at the same time.

It had already been confirmed that in cases of graphite materials the impact force, calculated by directly employing the Hertzian contact stiffness derived from eqn (2), was greater than that of the

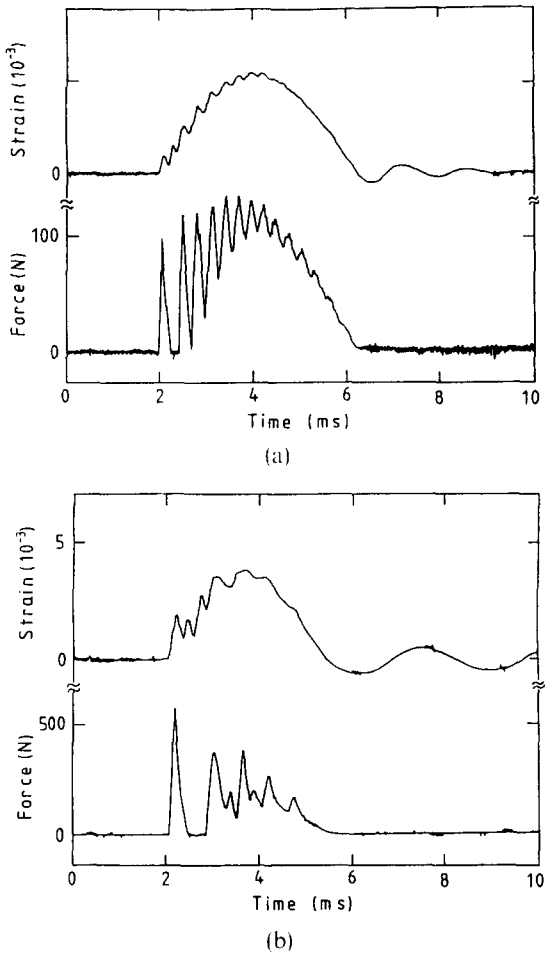

Fig. 3. Impact response waves. (a) *S*-Type specimen, impact velocity 0·6 m/s; (b) L-type specimen, impact velocity 2·0 m/s.

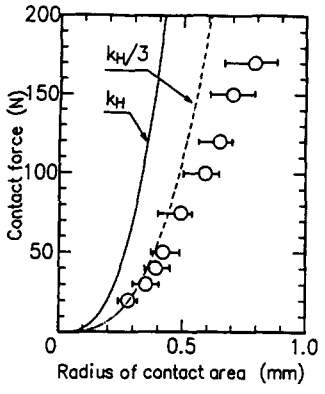

Fig. 4. Relation between contact force and radius of circular contact area in the *S*-type specimen of IG-11.

experimental result.[2,4,5] The deviation shows that a force–deformation relation at the contact area is not dependent on the elasticity because of the surface roughness of the specimen rod and the nonlinearity of the stress–strain relation in graphite materials, which is more conspicuous in a compressive region.[6] In the case where the radii of the cylinders are equal, the contact area becomes a circle, that is, a and b in eqns (4) and (5) are equal. Figures 4 and 5 show the relation between contact force and radius of a circular contact area in the *S*-type specimens of IG-11 and PGX. The solid line derived by eqns (4) and (5) is not suitable to represent the experimental results. The contact stiffness, therefore, was considered to be an adjustable value to describe the relations. It can be said from the figures that one third of k_H is sufficiently applicable to describe the relations within about 100 N of the contact force, irrespective of the kind of graphite. Accordingly, the Hertzian contact stiffness modified to be $k_H/3$ will be employed for the impact response analysis because most of the impact forces generated in the impact tests are less than 100 N.

Figure 6 shows the results of the impact response analysis using $k_H/3$ as the contact stiffness. The analytical results represent the experimental ones adequately where the high-frequency components are superimposed on the force and the stress. The

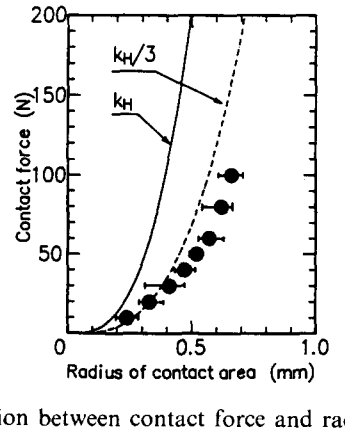

Fig. 5. Relation between contact force and radius of circular contact area in the *S*-type specimen of PGX.

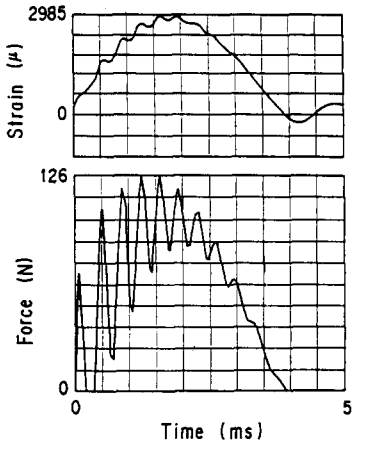

Fig. 6. Analytical results of impact response waves for *S*-type specimen, impact velocity 0·6 m/s.

agreement between the experimental and the analytical results is also confirmed in the case of PGX. It can be said, therefore, that the beam model having the modified Hertzian contact stiffness between specimen and tup is useful to describe the impact bending response of the graphite beam in which the high-frequency components are developed under impact loading.

4.2 Impact bending strength

In order to investigate the effect of the strain rate on the bending strength, impact and quasi-static bending tests were performed using the same material and size specimens as those in the fatigue test.

In the quasi-static test, the bending strain rate obtained from the gage fixed at the center of the specimen ranged from 10^{-5} to 10^{-6}/s. Figure 7 shows the Weibullian distributions for the bending strength obtained in the quasi-static test. Table 2 indicates the Weibull's parameters. It can be said for a Weibull plot having a straight-line portion as shown in Fig. 7 that the Weibull's function is applicable to describe not only the distribution of the strength of graphites in compression and tension[6] but also that in bending. The volume effect on the bending strength is not observed in the range of these specimen sizes.

Figure 8 illustrates the impact force and the strain

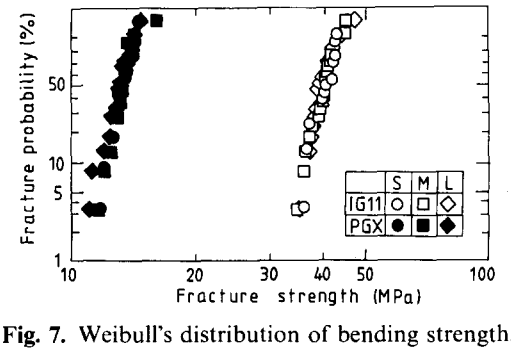

Fig. 7. Weibull's distribution of bending strength.

Table 2. Weibull's parameters

Weibull's parameter	*IG-11*			*PGX*		
	S	*M*	*L*	*S*	*M*	*L*
Number of specimens	19	20	20	20	20	20
Weibull's modulus	16·2	16·8	15·6	18·5	16·7	15·7
Mean value (MPa)	40·3	40·2	40·0	13·3	13·4	13·1

at fracture. In the impact test, the strain rate $\dot{\varepsilon}$ is approximately defined to be the strain at fracture ε_f divided by the time $(T_f - T_i)$. The strain rate is dependent on both the mass of the impact hammer and the specimen size and ranges from 1 to 5/s.

The relation between the fracture strain ε_f and the strain rate $\dot{\varepsilon}$ is shown in Fig. 9. Despite both the specimen size and the kind of graphite, it can be said that the fracture strain ε_f in bending is independent of the strain rate up to 5/s.

The relation between the bending strength and the strain rate is shown in Fig. 10. The bending strength is derived from the elastic theory of a beam assuming that the impact force acts on the specimen quasi-statically. The higher the impact velocity, the larger the dispersion of the strength becomes. That is because the effect of the superimposed high-frequency components on the impact force is magnified with increasing impact velocity. The bending strength, however, seems to be independent of the strain rate up to at least 5/s regardless of both the kind of graphite and the specimen size.

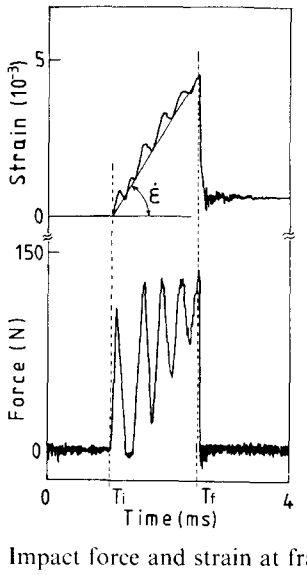

Fig. 8. Impact force and strain at fracture.

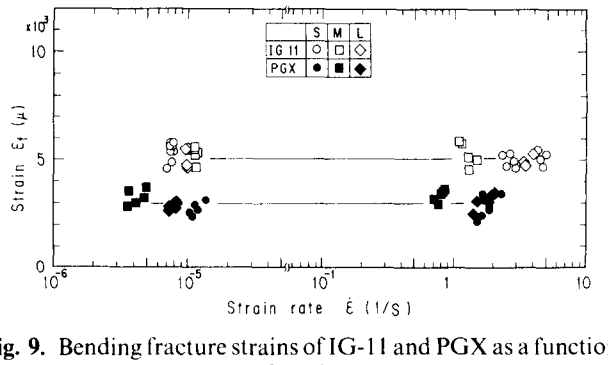

Fig. 9. Bending fracture strains of IG-11 and PGX as a function of strain rate.

4.3 Behavior of impact fatigue

4.3.1 Relation between impact energy and fatigue life

Figure 11 shows the relation between the impact energy U_i and the number of cycles to failure N_f (U–N diagram). The lines in the figure are derived from the following equation whose constants are determined by applying the least squares method to experimental data:

$$\log U_i = A + B \log N_f \tag{6}$$

It is revealed from U–N diagrams that despite the kind of graphite the larger the specimen size the longer its fatigue life is, and that the impact energy at failure in PGX is approximately a third of that in IG-11. Figure 12 shows the relation between the impact energy per unit volume U_i/V and N_f. Regardless of the specimen size the behavior of

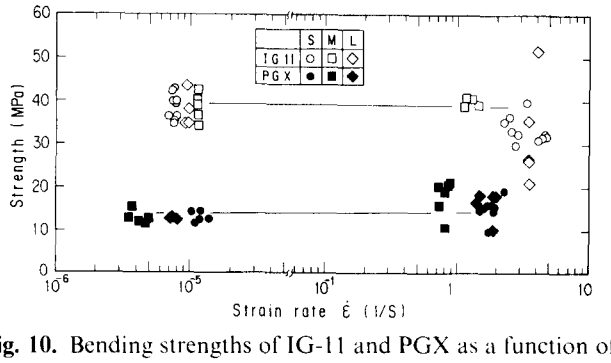

Fig. 10. Bending strengths of IG-11 and PGX as a function of strain rate.

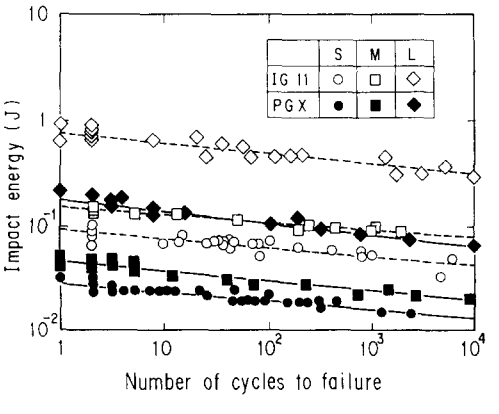

Fig. 11. U–N diagrams of IG-11 and PGX.

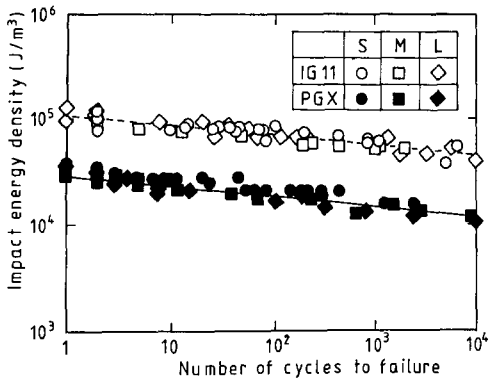

Fig. 12. U/V–N diagrams of IG-11 and PGX.

impact fatigue for IG-11 and PGX is described by each line which has almost the same inclination.

Assuming that the contact deformation under the point of impact is so small as to be ignored and the bending behavior of the specimen conforms to the elastic theory, generally, the elastic energy on bending is given by

$$U_e = \frac{\sigma_b^2 V g}{2E} \tag{7}$$

where V is the volume of specimen and g a factor to account for the stress distribution in the specimen ($g = 1/9$ for square-section bars in three-point bending and 1/12 for round-section bars), σ_b a bending stress and E the modulus of elasticity. Provided the impact energy is convertible into elastic energy, the stress generated by impact is proportional to the square root of U_i/V. Therefore, it is intimated through Fig. 12 that the stress generated by impact is valid to characterize the behavior of impact fatigue in the graphite materials tested here.

4.3.2 Comparison between impact and nonimpact fatigue

The behavior of nonimpact fatigue in each graphite (S–N diagram) is shown in Fig. 13. The ordinate in each S–N diagram denotes the normalized stress. That is, the maximum bending stress σ_{max} is normalized using the static bending strength of each graphite in order to compare the behavior of fatigue between IG-11 and PGX. The regression curves in Fig. 11 are given by

$$\log(\sigma_{max}/\sigma_s) = A + B \log N_f \tag{8}$$

It can be said from Fig. 13 that the normalized stress is valid to characterize the bending fatigue behavior of the graphites because the inclination of the regression curves is independent of both the kind of graphite and the specimen size.

It is necessary to transform the U–N diagram shown in Fig. 11 to the S–N diagram in order to compare the impact fatigue strength with the nonimpact one. Figures 14 and 15 show the relations

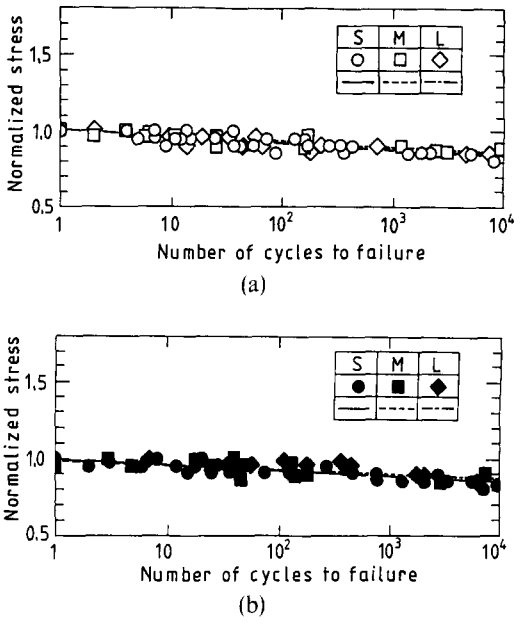

Fig. 13. Nonimpact fatigue behaviors of (a) IG-11 and (b) PGX.

of each graphite between $\sqrt{U}$ and the maximum stress σ_{max} generated by impact which is evaluated from the measured strain based on the elastic theory. It is clear that the stress is proportional to $\sqrt{U}$ and the slope of line depends on the specimen size. The solid lines denoting the analytical results obtained using the beam model are in adequate agreement with the experimental results. The broken lines indicate the results obtained from eqn (7). The reason why the slopes of the beam model are somewhat larger than that of eqn (7) is attributed to the application of the experimental damping effect to the beam model, while the energy loss is excluded in eqn (7).

Figure 16 shows the S–N diagram of impact fatigue transformed from the U–N diagram by using the relation between $\sqrt{U}$ and σ_{max} shown in Figs 14 and 15. The ordinate indicates the normalized stress and the regression curve is obtained from eqn (8). Despite the kind of graphite, the behavior of impact fatigue in each specimen size can almost be represented by an identical curve.

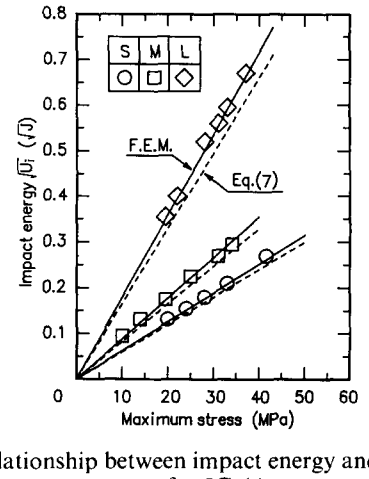

Fig. 14. Relationship between impact energy and impact stress for IG-11.

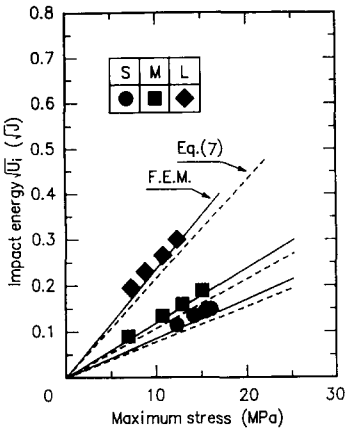

Fig. 15. Relationship between impact energy and impact stress for PGX.

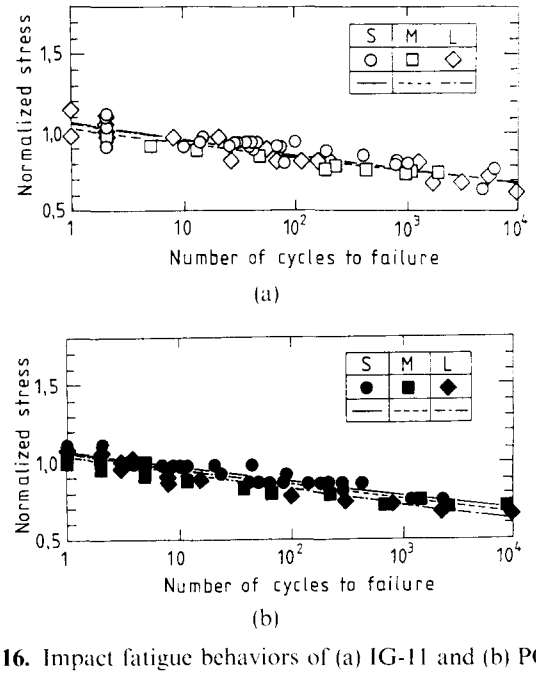

Fig. 16. Impact fatigue behaviors of (a) IG-11 and (b) PGX.

The regression curves of both impact and nonimpact fatigue are put together in Fig. 17. It can be said that the strength of graphite is lower in impact fatigue than in nonimpact fatigue, especially in the region of lower stress, irrespective of the kind of graphite and the specimen size.

The effect of the high-frequency components of the stress on the impact fatigue was evaluated assuming that fatigue damage was accumulated according to the modified Miner's rule based on the nonimpact bending fatigue. Two methods were employed to count the stress peaks on each cycle: one is to count a maximum peak and the other to count all peaks which seems to give the most conservative evaluation. Accordingly, the linear accumulation factors D_1, D_2 evaluated using the maximum peak and the all peaks count methods are given by

$$D_{1,2} = \sum_i \frac{n_{1i,2i}}{N_i} \tag{9}$$

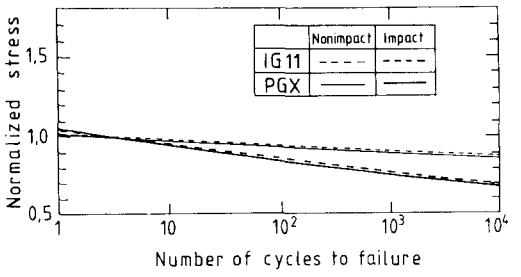

Fig. 17. Comparisons of fatigue strength in impact with that in nonimpact for IG-11 and PGX.

where N_i is the stress cycles in the nonimpact fatigue and $n_{1i,2i}$ is the stress cycles counting the maximum peak and the all peaks in the impact fatigue. Figure 18 shows D_1 and D_2. Because the discrepancy between D_1 and D_2 was hardly observed, the degradation of fatigue strength under impact loading can not be explained by considering the high-frequency components of the generated stress through the modified Miner's rule. The tendency is similar to those of many metals[7,8] and other graphites.[9] Recently, likewise, observations of fatigue crack initiation and propagation under impact loading have been made by some investigators, which show that crack growth rates become higher than under nonimpact loading[10-13] as well as the crack initiation being influenced by the rising rate of load and occurring earlier than under impact loading.[13] Accordingly, in order to evaluate the

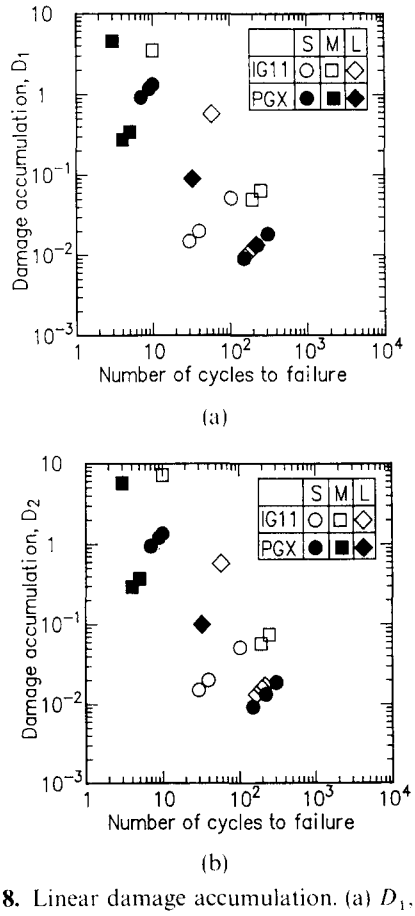

Fig. 18. Linear damage accumulation. (a) D_1, (b) D_2.

impact fatigue damage rigorously, it seems to be necessary to take account of the effects of not only the high-frequency components superimposed on the stress wave but also the strain rate on the fatigue strength under impact loading.

5 Conclusion

The bending strength tests were carried out under both impact and nonimpact loading on two kinds of graphite materials by using the pendulum-type repeatedly impacting machine. The beam model taking account of the contact stiffness through the Hertzian theory was applied to evaluate the relation between the impact energy, the impact force and the generated stress.

The following conclusions were obtained.

(1) The impact behavior of the graphite, such as the impact force, the bending stress and the contacting time, can be represented using the beam model with a modified Hertzian contact stiffness.

(2) The bending strength of the graphites is independent of the strain rate in the range from 10^{-6} to 5/s.

(3) The effect of specimen size on both the bending fatigue behavior and the bending strength was not observed in the experimental range.

(4) The maximum stress generated by impact is a unique variable to describe the endurance curve of impact fatigue behavior represented on the S–N diagram irrespective of the specimen size.

(5) It can be concluded from the S–N diagram that the fatigue strength of graphite is lower under impact loading than in nonimpact loading.

References

1. Present status of HTGR research and development. JAERI, 1990.
2. Futakawa, M., Kikuchi, K., Muto, Y. & Shibata, H., Impact bending fatigue and impact response behavior of a nuclear-grade graphite beam. *Carbon*, **28**(1) (1990) 149–54.
3. Goldsmith, W., *Impact*. Edward Arnold, London, 1960.
4. Darby, M. I., Calculations of impact stresses in polycrystalline graphite rods. *J. Mater. Sci.*, **19** (1984) 1930–8.
5. Evans, G. R., Jones, B. C., McMillan, A. J. & Darby, M. I., A new numerical method for the calculation of impact forces. *J. Phys. D: Appl. Phys.*, **24** (1991) 854–8.
6. Ishihara, M., Iyoku, T., Toyoda, J., Sato, S. & Shiozawa, S., An explication of design data of the graphite structural design code for core support components of high temperature engineering test reactor. JAERI-M 91-154, 1991.
7. Maekawa, I., Tanabe, Y., Nishida, S., Ashizawa, T. & Ogawa, H., Comparative study of impact fatigue with usual fatigue. *Trans. JSME*, **56**(525) (1990) 1051–7.
8. Tanaka, T. & Nakamura, H., On the impact fatigue strength of metallic materials. *J. Soc. Mater. Sci., Japan*, **23**(252) (1974) 678–85.
9. Birch, M. & Brocklehurst, J. E., The impact endurance of polycrystalline graphite. *Carbon*, **21**(5) (1983) 497–510.
10. Tanaka, T., Nakamura, H. & Kimura, K., On the impact fatigue crack growth behavior of metallic materials. *Fatigue Fract. Engng Mater. Struct.*, **8**(1) (1985) 13–22.
11. Murakami, R., Ito, K. & Akizono, K., On the fatigue crack propagation behavior under repeated impacts using a new type of impact fatigue testing machine. *J. Soc. Mater. Sci., Japan*, **33**(375) (1984) 1527–32.
12. Iguchi, H., Tanaka, K. & Taira, S., Failure mechanisms in impact fatigue of metals. *Fatigue Engng. Mater. Struct.*, **2** (1979) 165–76.
13. Maekawa, I., Tanabe, Y., Watanabe, H., Jin, Z. & Ogawara, Y., Growth of crack in steel by impact tension. *Trans. JSME* **52**(473) (1990) 249–56.